



HAL
open science

Gain-of-Function Mutations in RPA1 Cause a Syndrome with Short Telomeres and Somatic Genetic Rescue

Richa Sharma, Sushree Sahoo, Masayoshi Honda, Sophie Granger, Charnise Goodings, Louis Sanchez, Axel Künstner, Hauke Busch, Fabian Beier, Shondra Pruett-Miller, et al.

► **To cite this version:**

Richa Sharma, Sushree Sahoo, Masayoshi Honda, Sophie Granger, Charnise Goodings, et al.. Gain-of-Function Mutations in RPA1 Cause a Syndrome with Short Telomeres and Somatic Genetic Rescue. Blood, 2021, 10.1182/blood.2021011980 . hal-03451935

HAL Id: hal-03451935

<https://hal.science/hal-03451935>

Submitted on 26 Nov 2021

HAL is a multi-disciplinary open access archive for the deposit and dissemination of scientific research documents, whether they are published or not. The documents may come from teaching and research institutions in France or abroad, or from public or private research centers.

L'archive ouverte pluridisciplinaire **HAL**, est destinée au dépôt et à la diffusion de documents scientifiques de niveau recherche, publiés ou non, émanant des établissements d'enseignement et de recherche français ou étrangers, des laboratoires publics ou privés.



American Society of Hematology
 2021 L Street NW, Suite 900,
 Washington, DC 20036
 Phone: 202-776-0544 | Fax 202-776-0545
 editorial@hematology.org

Gain-of-Function Mutations in *RPA1* Cause a Syndrome with Short Telomeres and Somatic Genetic Rescue

Tracking no: BLD-2021-011980R3

Richa Sharma (St Jude Children's Research Hospital, United States) Sushree Sahoo (St Jude Children's Research Hospital, United States) Masayoshi Honda (University of Iowa, United States) Sophie Granger (University of Iowa, United States) Charnise Goodings (St. Jude Children's Research Hospital, United States) Louis Sanchez (Sorbonne Université, Germany) Axel Künstner (University of Lübeck, Germany) Hauke Busch (University of Luebeck, Germany) Fabian Beier (University Hospital Aachen, Germany) Shondra Pruett-Miller (St. Jude Children's Research Hospital, United States) marcus Valentine (St Jude Children's Research Hospital, United States) Alfonso Fernandez (St Jude Children's Research Hospital, United States) Ti-Cheng Chang (St. Jude Children's Research Hospital, United States) Vincent Géli (U1068 Inserm, UMR7258 CNRS, Aix-Marseille University, Institut Paoli-Calmettes, France) Dmitri Churikov (Marseille Cancer Research Center, France) Sandrine Hirschi (Strasbourg University Hospital, University of Strasbourg, France) Victor Pastor (St Jude Children's Research Hospital, United States) Melanie Boerries (German Cancer Consortium (DKTK), Germany) Melchior Lauten (University Hospital Schleswig-Holstein, Campus Lübeck, Germany) Charikleia Kelaidi (Aghia Sophia Children's Hospital, Greece) Undiagnosed Network (,) Megan Cooper (Washington University, United States) Sarah Nicholas (Baylor College of Medicine, United States) Jill Rosenfeld (Baylor College of Medicine, United States) Sophia Polychronopoulou (Aghia Sophia Children's Hospital, Greece) Caroline Kannengiesser (APHP, Hopital Xavier Bichat, Service de Génétique, France) Carole Saintome (Muséum National d'Histoire Naturelle, France) Charlotte Niemyer (German Cancer Consortium (DKTK), German Cancer Research Center (DKFZ), Germany) Patrick Revy (Imagine Institute for Genetic Diseases, France) Marc Wold (University of Iowa, United States) Maria Spies (University of Iowa, United States) Miriam Erlacher (German Cancer Consortium (DKTK), German Cancer Research Center (DKFZ),) Stéphane Coulon (Marseille Cancer Research Centre, U1068 INSERM, UMR7258 CNRS, UM105 Aix-Marseille University, Institut Paoli-Calmettes,, France) Marcin Wlodarski (University of Freiburg, Germany)

Abstract:

Human telomere biology disorders (TBD)/short telomere syndromes (STS) are heterogeneous disorders caused by inherited loss-of-function mutations in telomere-associated genes. Here, we identify three germline heterozygous missense variants in *RPA1* gene in four unrelated probands presenting with short telomeres and varying clinical features of TBD/STS including bone marrow failure, myelodysplastic syndrome, T- and B-cell lymphopenia, pulmonary fibrosis, or skin manifestations. All variants cluster to DNA binding domain A of *RPA1* protein. *RPA1* is a single-strand DNA-binding protein required for DNA replication and repair and involved in telomere maintenance. We showed that *RPA1*^{E240K} and *RPA1*^{V227A} proteins exhibit increased binding to single-strand and telomeric DNA, implying a gain in DNA-binding function while *RPA1*^{T270A} has binding properties similar to wild type protein. To study the mutational effect in a cellular system, we used CRISPR/Cas9 to knock-in the *RPA1*^{E240K} mutation into healthy inducible pluripotent stem cells. This resulted in severe telomere shortening and impaired hematopoietic differentiation. Furthermore, in patient with *RPA1*^{E240K}, we discovered somatic genetic rescue (SGR) in hematopoietic cells due to an acquired truncating *cis* *RPA1* mutation or a uniparental isodisomy 17p with loss of mutant allele, coinciding with stabilized blood counts. Using single-cell sequencing, the two SGR events were proven to be independently acquired in hematopoietic stem cells. In summary, we describe the first human disease caused by germline *RPA1* variants in individuals with TBD/STS.

Conflict of interest: No COI declared

COI notes:

Preprint server: No;

Author contributions and disclosures: RS, SSS, MWW, CS, SC, MSW, MS conceived and designed the experiments. RS, SSS, AK, HB, TCC, MB, VPL, JAR, CK, MWW performed genomic data analysis. RS, MH, SLG, CG, LS, FB, MBV, SMPM, AGF, DC, VG, CS, PR, MSW, MS, and SC performed and/or interpreted functional experiments. FB, SH, ML, CK, MC, SN, JAR, SP, CMN, ME, RS, MWW were involved in patient care, collecting clinical data and clinical testing. MWW, SC, MSW, MS supervised the experiments, and MWW oversaw study design. All authors contributed to the manuscript and approved of the final version.

Non-author contributions and disclosures: No;

Agreement to Share Publication-Related Data and Data Sharing Statement: We are currently in the process of submitting all sequencing files to EGA archive (EGA box 1017)

Clinical trial registration information (if any):

Gain-of-Function Mutations in RPA1 Cause a Syndrome with Short Telomeres and Somatic Genetic Rescue

Richa Sharma^{1,#}, Sushree S. Sahoo^{1,#}, Masayoshi Honda², Sophie L. Granger², Charnise Goodings¹, Louis Sanchez^{3,4}, Axel Künstner⁵, Hauke Busch⁵, Fabian Beier⁶, Shondra M. Pruettt-Miller⁷, Marcus B. Valentine⁸, Alfonso G. Fernandez¹, Ti-Cheng Chang⁹, Vincent Géli¹⁰, Dmitri Churikov¹⁰, Sandrine Hirschi¹¹, Victor B. Pastor⁹, Melanie Boerries^{12,13}, Melchior Lauten¹⁴, Charikleia Kelaidi¹⁵, Undiagnosed Disease Network[&], Megan A. Cooper¹⁶, Sarah Nicholas¹⁷, Jill A. Rosenfeld¹⁸, Sophia Polychronopoulou¹⁵, Caroline Kannengiesser¹⁹, Carole Saintomé^{3,4}, Charlotte M. Niemeyer^{13,20}, Patrick Revy²¹, Marc S. Wold², Maria Spies², Miriam Erlacher^{13,20}, Stéphane Coulon¹⁰, Marcin W. Wlodarski^{1,20*}

¹Department of Hematology, St. Jude Children's Research Hospital, Memphis, TN, USA

²Department of Biochemistry, Carver College of Medicine, University of Iowa, Iowa City, IA, USA

³Structure et Instabilité des Génomes, Muséum National d'Histoire Naturelle, CNRS UMR 7196, INSERM U1154, 43 rue Cuvier, F-75005, Paris, France

⁴Sorbonne Université, UFR927, F-75005, Paris, France

⁵Lübeck Institute of Experimental Dermatology and Institute of Cardiogenetics, University of Lübeck, Lübeck, Germany

⁶Department of Hematology, Oncology, Hemostaseology and Stem Cell Transplantation, Medical Faculty, RWTH Aachen University, Aachen, Germany

⁷Department of Cell and Molecular Biology, St. Jude Children's Research Hospital, Memphis, TN, USA

⁸Cytogenetics Core Facility, St. Jude Children's Research Hospital, Memphis, TN

⁹Center for Applied Bioinformatics, St. Jude Children's Research Hospital, Memphis, TN 38105, USA

¹⁰Marseille Cancer Research Centre, U1068 INSERM, UMR7258 CNRS, UM105 Aix-Marseille University, Institut Paoli-Calmettes, Equipe labellisée par la Ligue Nationale contre le Cancer, Marseille, F-13009, France

¹¹Department of Respiratory Medicine and Rare Pulmonary Diseases, Strasbourg University Hospital, Strasbourg, France

¹²Institute of Medical Bioinformatics and Systems Medicine, Medical Center-University of Freiburg, Faculty of Medicine, University of Freiburg, Freiburg, Germany

¹³German Cancer Consortium (DKTK), Freiburg, Germany and German Cancer Research Center (DKFZ), Heidelberg

¹⁴University Hospital Schleswig-Holstein, Department of Pediatrics, University of Lübeck, Germany

¹⁵Department of Pediatric Hematology/Oncology, Aghia Sophia Children's Hospital, Athens, Greece

¹⁶Department of Pediatrics, Washington University School of Medicine, St. Louis, MO, USA

¹⁷Department of Allergy and Immunology, Baylor College of Medicine, Houston, TX, USA

¹⁸Department of Molecular and Human Genetics, Baylor College of Medicine, Houston, TX, USA

¹⁹Department of Genetics, Bichat Hospital, Assistance Publique - Hôpitaux de Paris, Paris University, INSERM U1152, Paris, France

²⁰Division of Pediatric Hematology and Oncology, Department of Pediatrics and Adolescent Medicine, Medical Center, University of Freiburg, Freiburg, Germany

²¹Université de Paris, Imagine Institute, Laboratory of Genome Dynamics in the Immune System, Laboratoire labellisé Ligue, INSERM UMR 1163, F-75015, Paris, France

Equal contribution

& Full contributor list of the Undiagnosed Disease Network in the supplement

*Corresponding author:

Marcin W. Wlodarski, MD, PhD

St. Jude Children's Research Hospital

262 Danny Thomas Place, MS 341

Memphis, TN 38105

Phone: 901-595-2484, Fax: 901-595-2176

E-mail: marcin.wlodarski@stjude.org

Running title: RPA1 in human disease

Article type: Regular article

Abstract: 222, Main text: 3993 words

Keywords: RPA1, telomeres, DNA binding, telomere biology disorder, short telomere syndrome

Key points:

- Germline *RPA1* gain-of-function missense mutations result in a telomere biology disorder phenotype
- Somatic rescue events arise in hematopoiesis secondary to germline *RPA1* mutation

58 **ABSTRACT**

59 Human telomere biology disorders (TBD)/short telomere syndromes (STS) are heterogeneous disorders
60 caused by inherited loss-of-function mutations in telomere-associated genes. Here, we identify three
61 germline heterozygous missense variants in *RPA1* gene in four unrelated probands presenting with short
62 telomeres and varying clinical features of TBD/STS including bone marrow failure, myelodysplastic
63 syndrome, T- and B-cell lymphopenia, pulmonary fibrosis, or skin manifestations. All variants cluster to
64 DNA binding domain A of RPA1 protein. RPA1 is a single-strand DNA-binding protein required for DNA
65 replication and repair and involved in telomere maintenance. We showed that RPA1^{E240K} and RPA1^{V227A}
66 proteins exhibit increased binding to single-strand and telomeric DNA, implying a gain in DNA-binding
67 function while RPA1^{T270A} has binding properties similar to wild type protein. To study the mutational
68 effect in a cellular system, we used CRISPR/Cas9 to knock-in the *RPA1*^{E240K} mutation into healthy
69 inducible pluripotent stem cells. This resulted in severe telomere shortening and impaired
70 hematopoietic differentiation. Furthermore, in patient with *RPA1*^{E240K}, we discovered somatic genetic
71 rescue (SGR) in hematopoietic cells due to an acquired truncating *cis RPA1* mutation or a uniparental
72 isodisomy 17p with loss of mutant allele, coinciding with stabilized blood counts. Using single-cell
73 sequencing, the two SGR events were proven to be independently acquired in hematopoietic stem cells.
74 In summary, we describe the first human disease caused by germline *RPA1* variants in individuals with
75 TBD/STS.

76 **INTRODUCTION**

77 Telomeres are complex structures made up of repetitive DNA sequences associated with specialized
78 proteins found at natural ends of linear chromosomes in all mammals. The hallmark function of
79 telomeres is to protect chromosomal ends from degradation and inappropriate recombination, and
80 activation of the DNA damage response¹. In the absence of telomere-associated proteins, chromosomal
81 ends undergo premature attrition with pathological consequence of telomere biology disorders (TBD),
82 also referred to as short telomere syndromes (STS) or dyskeratosis congenita. TBD/STS are hereditary
83 disorders that manifest on a wide phenotypic and age spectrum because of genetic heterogeneity and
84 variable expressivity. TBD/STS associated features include bone marrow failure (BMF), pulmonary and
85 liver fibrosis, mucocutaneous fragility, and predisposition to myelodysplastic syndromes (MDS) and
86 cancer²⁻⁵. Monoallelic or biallelic inactivation in 14 genes that code for telomerase holoenzyme,
87 shelterin complex, telomere capping machinery, and accessory telomere processes, have been identified
88 to cause TBD/STS^{2,6}. However, an estimated 30% of individuals with TBD/STS do not have a genetic
89 resolve, which obscures timely diagnosis and clinical management⁶.

90 Replication Protein A (RPA) is a ubiquitous, single-strand (ss) DNA binding protein that exists as a
91 heterotrimer complex composed of RPA1, RPA2 and RPA3 in eukaryotes⁷. RPA is essential for DNA
92 replication and repair. It binds all ssDNA sequences with high affinity to provide nuclease protection,
93 prevent hairpin formation and recruit numerous proteins to facilitate ssDNA processing and repair.
94 Importantly, RPA is involved in several DNA damage signaling and repair pathways including nucleotide
95 excision repair, base excision repair, mismatch repair, and double strand break repair⁸⁻¹¹. RPA1, the
96 largest subunit of RPA, harbors four DNA binding domains (DBD, -F, -A, -B, -C) of which DBD-A and DBD-
97 B are important for high affinity ssDNA binding and facilitating protein-protein interactions^{12,13}. Despite
98 no clear association with human disease, the ubiquitous involvement of RPA1 in genome integrity and
99 the demonstrated overexpression in some cancers¹⁴⁻¹⁷ has driven research efforts to understand its
100 functions. Thus far, only loss-of-function (LOF) *RPA1* alleles have been identified through mutagenic
101 screens in eukaryotic systems¹⁸⁻²⁰. Disrupted DNA repair and chromosomal rearrangements were shown
102 in yeast and human cell lines¹⁸⁻²⁰ while genomic instability and tumorigenesis were demonstrated in
103 mice^{21,22}. Studies in yeast revealed that RPA complex binds to telomeric regions during S-phase and
104 unfolds G-quadruplex (G4) secondary DNA structures enriched at telomeres²³⁻²⁸. Furthermore, *RPA1*
105 mutants were associated with telomere shortening in yeast models and cell lines^{24,25,27,29-32}. However,
106 the mechanism of how *RPA1* genetic disruption affects telomere length is not well understood.

107 *RPA1* mutations have not yet been reported in human syndromes. Here, we describe three germline
108 heterozygous missense variants in *RPA1* in four unrelated individuals with short telomeres and
109 phenotypes seen in TBD/STS, including hematologic, pulmonary, and skin manifestations. Biochemical
110 studies revealed that these mutants have core DNA-binding domains with elevated affinity, pointing to a
111 unique gain-of-function (GOF) effect for at least two of the mutants studied, while cellular studies show
112 defective hematopoiesis with telomere shortening in *RPA1*-mutated iPSCs. Finally, we found
113 independent acquired somatic rescue events in one patient, resulting in inactivation of the germline
114 *RPA1* mutation.

115 MATERIAL AND METHODS

116

117 Patient cohort

118 This study was approved by the institutional review boards of the respective institutions (St. Jude
119 Children's Hospital, INSIGHT-HD; University of Freiburg, CPMP/ICH/135/95 and 430/16; Baylor College of
120 Medicine, H-34433; HUPNVS, Paris 7 University, AP-HP, IRB 00006477). Written informed consent was
121 obtained from patients or guardians. Patient 1 (P1) and patient 2 (P2) were enrolled in the observational
122 study of the European Working Group for MDS in Childhood (EWOG-MDS, (NCT00662090). Patient (P3)
123 had an institutional diagnosis of idiopathic pulmonary fibrosis (IPF) and was enrolled at Paris 7
124 University, AP-HP, IRB 00006477. Patient 4 (P4) was enrolled in Undiagnosed Disease Network (UDN)
125 (NIH IRB 15HG0130). Peripheral blood, bone marrow, fibroblasts, and hair follicles were collected from
126 patients and family members when available.

127

128 Whole exome sequencing

129 Whole exome sequencing (WES) was performed on the genomic DNA of bone marrow and peripheral
130 blood cells of P1-P4 and family members (P1: parents and unaffected brother, P2: parents and
131 unaffected sister, P4: parents). Standard WES sequencing and analytic approaches were applied. In
132 detail, TruSeq DNA Exome kit (Illumina, cat no. 20020615), SureSelect V5 (Agilent, cat no. 5190-6209),
133 and Human Comprehensive Exome (TWIST Biosciences) were used for enrichment and library
134 preparation according to the manufacturers' instructions. The generated libraries were sequenced on
135 the Illumina HiSeq 2500 with 150-bp paired-end reads and average 50-100x coverage. After
136 demultiplexing, the FASTQ files were trimmed for adapter sequences and mapped either to
137 GRCh38/hg38 (P1_quartet) or GRCh37/hg19 (P2_quartet, P3, P4_trio) using BWA MEM (v0.7.15). The
138 mapping data from P1_trio, P2_quartet, and P3 were post-processed according to GATK best practices
139 (GATK v4.1.7; SAMtools and PICARD v 2.23.0), and variant calling (single nucleotide variants and short
140 insertions/deletions) was performed by applying GATK Haplotypecaller v4 for P1_trio and P3, and
141 DeepVariant (v1.1.0; ES mode) for P2_quartet. The called variants were then annotated using ANNOVAR
142 for P1_trio and variant effector predictor (VEP, v100) for P2_quartet. While for P3, the variants
143 annotation and filtering process was performed using the Polyweb software interface of the
144 Bioinformatic department of Imagine Institute, Paris. Finally, for P4_trio, the mapping, processing,
145 variant calling, annotation, and filtering was achieved using the Baylor College of Medicine institutional
146 pipeline³³. After mapping, variant calling and annotation, we used a single stringent filtering approach to
147 establish a list of rare candidate variants fulfilling the following criteria: 1) minor allelic frequency (MAF)

148 below 0.01% in gnomAD population database, 2) minimum 6 altered forward and reverse reads, 3)
149 exonic non-synonymous variant effect, and 4) CADD score greater than 20. Altogether, this resulted in
150 the discovery of *RPA1* variants reported in this study.

151

152 **Single-cell DNA and protein sequencing**

153 Single-cell DNA sequencing (scDNaseq) of bone marrow (BM) cells was performed using a custom
154 targeted panel on the Tapestry platform (MissionBio). Briefly, a set of amplicons including *RPA1* variants
155 found in P1 (germline c.718G>A, chr17:1782314:G>A and somatic c.1735G>T, *RPA1*:chr17:1798378:G>T)
156 were amplified as previously reported³⁴, and outlined in detail in the supplement. In addition, we used
157 oligonucleotide-conjugated antibodies targeting CD3, CD11b, CD19, CD34, CD38, CD45RA, and CD90 cell
158 surface proteins.

159

160 **Data availability**

161 Python-based Mosaic package for analysis of scDNA sequencing is available at GitHub
162 (<https://github.com/MissionBio/mosaic>). Raw datasets of whole exome sequencing and scDNaseq have
163 been deposited at the European Genome-Phenome Archive (EGA, <http://www.ebi.ac.uk/ega/>) hosted by
164 the European Bioinformatics Institute under accession numbers EGAS00001005761 (WES) and
165 EGAS00001005762 (single cell DNA sequencing and cell-surface protein analysis).

166

167 Additional methods are outlined in detail in the supplement: telomere length assessment (Q-FISH,
168 Southern blot, Flow-FISH, TeSLA); biochemical studies of *RPA1* variants (expression, purification, Förster
169 resonance energy transfer (FRET)); iPSC model (CRISPR/Cas9 targeted mutagenesis, quality assessment,
170 hematopoietic differentiation, cytospins, protein expression, irradiation and assessment of DNA
171 damage, flow cytometry); genomics (deep sequencing, bone marrow derived single colony sequencing,
172 RNA sequencing, *RPA1* allelic quantification, digital droplet PCR, SNP arrays, haplotype phasing and
173 quantification of uniparental isodisomy, Sanger sequencing); and statistics.

174 **RESULTS**175 **Heterogenous clinical manifestations of TBD/STS unified by short telomeres in the study cohort**

176 In the process of identifying new genetic causes of Mendelian disorders, we compiled an international
177 cohort of four patients with phenotype consistent with TBD/STS and yet unidentified genetic cause
178 (Table 1, Fig. 1A). All patients' medical records and evaluations underwent central review and had
179 negative workup for inherited BMF syndromes and TBD/STS associated genes. Unbiased WES found
180 three germline heterozygous missense variant alleles in *RPA1* (NM_002945.5) as the most plausible
181 candidates in our patient cohort (Table 1, Fig. 1A). *De novo RPA1* c.718G>A, p.E240K and c.808A>G,
182 p.T270A occur in P1 and P4, respectively and are previously unreported in population or disease
183 databases. *RPA1* c.680T>C, p.V227A variant found in P2 and P3 occurs at ultra-low frequency in control
184 populations (Table 1). P2 father and sister are carriers without history of hematologic manifestations
185 (clinical workup declined) and P3 family members were not available for evaluation. We did not identify
186 other *de novo* variants in genes involved in hematopoiesis, telomere homeostasis, or cancer that would
187 be compatible with the observed phenotypes. All *de novo* variants in P1, P2, and P4 are shown in
188 Supplemental Table 1. *RPA1* is located on chromosome 17p13.3 and has 17 coding exons coding for a
189 70kDa protein that is expressed in all tissues (Fig. 1B, top panel). The three *RPA1* variants cluster to DNA
190 binding domain A (DBD-A) of RPA1 protein (Fig. 1B, bottom panel) and are near ssDNA binding grooves
191 (Supplemental Fig. 1A). These variants affect semi to highly conserved nucleotides (Supplemental Fig.
192 1B) with resulting amino acid substitutions predicted as likely deleterious (Table 1).

193
194 Our patient cohort had a broad spectrum of clinical presentation and age of onset. P1 presented at age
195 10 years with pancytopenia, hypoplastic BM (Fig. 1C) and history of congenital eye anomaly requiring
196 enucleation as an infant (Table 1). She further developed classic dyskeratosis congenita associated
197 mucocutaneous triad during adolescence (Fig. 1C). However, her clinical course was atypical due to
198 stabilization of blood counts and mucocutaneous features (Fig. 1C) without intervention over 18 years.
199 P2, with pre-existing facial dysmorphisms (Table 1), was diagnosed at 13 years of age with MDS with
200 excess blasts (Fig. 1C) and somatic *NRAS* c.35G>A, p.G12D mutation at 37% allelic frequency. Mild
201 restriction was noted on pulmonary function testing prior to receiving myeloablative allogeneic
202 hematopoietic stem cell transplantation (HSCT). Short-term complications of HSCT included severe skin
203 and liver graft versus host disease (GVHD) with development of necrotizing pneumonitis with extensive
204 cavitation (Fig. 1C) secondary to multifactorial cause including pulmonary GVHD, infections (nocardia
205 pneumonitis, pulmonary aspergillosis) and pulmonary fibrosis at 8 months post-HSCT. Patient passed
206 away 11 months post-HSCT of multi-organ failure in setting of subarachnoid hemorrhage and intractable

207 chronic GVHD. P3 had early hair graying and adult-onset IPF that progressed in her 5th decade of life
208 (Table 1, Fig. 1C). Two siblings of P3 were also diagnosed with IPF but genetic studies to segregate *RPA1*
209 mutation were not possible due to death caused by IPF-related complications (Supplemental Fig. 2). P4
210 presented at birth with prematurity, failure to thrive and low T-cell receptor excision circles, triggering
211 further workup that was significant for T- and B-cell lymphopenia and severe hypogammaglobulinemia
212 requiring chronic replacement therapy (Supplemental Table 2). Due to clinical features consistent with
213 TBD/STS disease spectrum, we assessed telomere length in all patients using different standard
214 approaches depending on specimen availability. P1 and P4 had decreased telomere length in peripheral
215 blood lymphocytes compared to age-matched controls (Fig. 1D) using flow FISH³⁵. Specifically, P1 had
216 telomere length < 1st percentile measured at two time points three years apart while P4 telomere length
217 decreased to <1st percentile from 5th percentile over 1.5 years. Telomere restriction fragment (TRF)
218 analysis on DNA from peripheral blood of P2 and P3 revealed short telomeres in P2 compared to family
219 members, as well as, in P3 compared to age-matched healthy control (Fig. 1E). To gain further
220 resolution, TeSLA assay was performed in blood DNA, showing higher proportion of telomeres less than
221 1 kilobase (kb) in P2 and P3 (Supplemental Fig. 3A-B), consistent with increased frequency of very short
222 telomeres.

223

224 **Germline *RPA1* variants exhibit increased binding to ssDNA and telomeric DNA**

225 To assess the effects of human *RPA1* variants on RPA heterotrimer formation and function (Fig. 2A), we
226 expressed and purified RPA heterotrimers with wild type *RPA1* (RPA^{WT}) and mutant V227A (RPA^{V227A}),
227 E240K (RPA^{E240K}) and T270A (RPA^{T270A}) proteins (Supplemental Fig. 4A). All proteins did form
228 heterotrimers and bound ssDNA with high affinity in a FRET based DNA-binding assay using Cy3/Cy5-
229 labeled dT30 ssDNA (Fig. 2B). All three mutant proteins appear to form an altered complex with ssDNA.
230 Each saturates dT30 ssDNA at a lower stoichiometry than wild type: the binding ratio was 2.2 for RPA^{WT} ,
231 1.3 for RPA^{V227A} , 1.1 for RPA^{E240K} , and 1.6 for RPA^{T270A} (Fig. 2B, Supplemental Table 3). We next examined
232 *RPA* binding to dT15, which only interacts with DBD-A and DBD-B of *RPA1*. Compared to RPA^{WT} , RPA^{V227A}
233 and RPA^{E240K} displayed a two-fold and eight-fold higher affinity, respectively, while RPA^{T270A} had a
234 marginally higher (1.3-fold) binding (Fig. 2C, Supplemental Table 3). When assessing for binding to 15-
235 mer human telomeric sequence (TTAGGG)₂TTA, RPA^{V227A} and RPA^{E240K} had increased binding affinity
236 while RPA^{T270A} had no effect compared to RPA^{WT} (Fig. 2D, Supplemental Table 3). Next, we examined the
237 kinetics of the telomeric G-quadruplexes (h-telG4) melting (Fig. 2E and 2F, Supplemental Fig. 4B-E,
238 Supplemental Table 3). RPA^{E240K} and RPA^{V227A} showed a greater extent (Fig. 2E) and rate of melting of h-
239 telG4 sequences (Fig. 2F) versus RPA^{WT} , especially at sub-saturating protein concentrations. We

240 conclude that all three mutants have a high affinity for DNA and RPA^{V227A} and RPA^{E240K} exert a higher
241 affinity and telomere unfolding capacity than RPA^{WT}.

242

243 ***RPA1*^{E240K} mutation results in premature telomere shortening and abnormal hematopoiesis in an iPSC** 244 **model**

245 To understand the effect of *RPA1* variants on telomere length regulation and hematopoiesis (Fig. 3A),
246 we used CRISPR/Cas9-mediated mutagenesis to introduce homozygous E240K variant (denoted as
247 *RPA1*^{E240K}) into the endogenous *RPA1* locus of a healthy female donor iPSC line (*RPA1*^{WT}). *RPA1* whole
248 gene sequencing and Sanger analysis (Fig. 3A) confirmed on-target mutagenesis. *RPA1*^{WT} and *RPA1*^{E240K}
249 iPSC lines had similar *RPA1* protein expression (Fig. 3B), normal karyotype (Supplemental Fig. 5A) and
250 intact pluripotency (Supplemental Fig. 5B). Given the role of *RPA1* in replication and DNA repair, we
251 assessed baseline cell cycle and activation of DNA damage response to irradiation, which showed similar
252 cell cycle profiles and γ -H2AX signaling in both *RPA1*^{WT} and *RPA1*^{E240K} iPSCs (Supplemental Fig. 6A-B). We
253 then measured telomere length using Q-FISH (Fig. 3C, Supplemental Fig. 6C) and TRF (Supplemental Fig.
254 6D), which revealed significantly shorter telomeres in *RPA1*^{E240K} compared to *RPA1*^{WT} iPSC independent
255 of cell passage. Significant telomere length reduction was also observed in *RPA1*^{E240K} iPSC-derived HP
256 (Fig. 3D). To assess whether *RPA1*^{E240K} affects hematopoiesis and whether *RPA1*^{E240K} iPSC model could
257 faithfully recapitulate P1 phenotype of pancytopenia, we evaluated iPSC-derived hematopoietic
258 differentiation with flow cytometric enumeration of cell subsets (Supplemental Fig. 7). Consistent with
259 reduced hematopoietic potential, *RPA1*^{E240K} iPSC yielded lower percentage of cells with CD43⁺CD45⁺
260 hematopoietic phenotype compared to *RPA1*^{WT} (Fig. 3E). Differentiation of HP cells (CD34⁺CD43⁺) to
261 terminal lineages was also compromised. Specifically, *RPA1*^{E240K} produced significantly less CD71⁺CD235⁺
262 erythroid (Fig. 3F) and CD45⁺CD18⁺CD11b⁺ myeloid populations (Fig. 3G) with cytological evidence of
263 scarce orthochromatic proerythroblasts (Supplemental Fig. 8A-B) and large macrophage-like cells,
264 respectively (Supplemental Fig. 8C-D).

265

266 **Somatic inactivation of germline *RPA1* mutation results in benign clonal hematopoiesis with long-term** 267 **potential**

268 The atypical clinical course in P1 with stable blood counts over two decades (Fig. 4A) without
269 progression of leukoplakia (Fig. 1C) and telomere shortening (Fig. 1D) led us to examine patient
270 specimens for potential rescue mechanisms. We found that allelic frequency of *RPA1* c.718G>A, p.E240K
271 variant is reduced in BM (27%) compared to fibroblast DNA (50%) (Fig. 4B). Two somatic events were
272 identified in BM: a second-site truncating (stop-gain) *RPA1* mutation c.1735G>T, p.K579* at 10% allelic

273 frequency (Fig. 4B) and a uniparental isodisomy of chromosome 17p (UPD17p) (Fig. 4C). To understand
274 the mechanism of these rescue events, we first confirmed the stop-gain c.1735G>T mutation to be *in cis*
275 with germline c.718G>A allele (Fig. 4D, Supplemental Fig. 9). Bulk RNA sequencing of BM cells revealed
276 total loss of the somatic mutation concurrent with reduction of germline variant to 13% (Fig. 4B).
277 Ultradeep RNA sequencing performed to accurately quantify these mutations confirmed nearly absent
278 expression (0.8%) of somatic c.1735G>T substitution (Fig. 4E). To assess whether the two mosaic events
279 were sustained over time, we performed serial SNP-array and deep sequencing of hematopoietic cells.
280 We also demonstrated a significant expansion of UPD17p clone over 15 years (Fig. 4C) which
281 corresponds to the declining germline c.718G>A allele on serial BM evaluations (Fig. 4F). In addition, we
282 observed an independent increase in clonal burden of somatic c.1735G>T, p.K579* mutation over time
283 (Fig. 4F).

284

285 **Analysis of clonality at single-cell resolution identifies mutually exclusive rescue events that arise in** 286 **early hematopoiesis**

287 To dissect the clonal architecture at single cell level, we interrogated P1 BM using scDNAseq. Three
288 clones with unique *RPA1* allelic patterns were detected at age 13 years: heterozygous c.718G>A (native
289 state hematopoiesis), homozygous wild type (rescue clone 1 with UPD17p), and heterozygous c.718G>A
290 with concurrent somatic c.1735G>T (rescue clone 2 with stop-gain mutation) (Fig. 4G). This clonal
291 pattern was confirmed in hematopoietic progenitor colonies derived from BM (Supplemental Fig. 10A).
292 Clonal trajectories assessed over 4 years demonstrated minor expansion of rescue clone 2 at the
293 expense of native hematopoiesis (Fig. 4G). Finally, we investigated clonal origins within hematopoietic
294 hierarchy by using barcoded antibodies in the same reaction to track surface markers on single cell level.
295 Both rescue clones were found within hematopoietic stem and progenitor cells (HSPC) characterized by
296 the expression of CD34, CD90, and CD38 (Fig. 4H). In addition, compared to native hematopoiesis, these
297 clones were enriched in CD11b⁺ myeloid and CD19⁺ B-cells but markedly reduced in CD3⁺ T-lymphocytes
298 (Fig. 4H). Similar skewing of UPD17p lesion towards myeloid lineage was observed comparing SNP arrays
299 results in bulk granulocytes versus lymphocytes (Supplemental Fig. 10B). The enrichment of both
300 somatic clones in CD11⁺ and CD19⁺ cells with a near absence of rescue hematopoiesis in T-lymphocytes
301 (Fig. 4H) is likely due to their long lifespan compared to short-lived myeloid and B-cell lineages. Of note,
302 no malignant somatic alterations (i.e. CHIP mutations) were found using WES in BM after diagnosis.

303 **DISCUSSION**

304 It was not until the late 20th century that *DKC1* was identified as the first gene to cause dyskeratosis
305 congenita, a syndrome described in 1910 with features of nail dystrophy, oral leukoplakia and skin
306 pigmentation anomalies³⁶. Since then, an increasing number of genes involved in telomere homeostasis
307 have been associated with classical phenotypes of TBD/STS which include BMF and mucocutaneous
308 triad, but also manifestations such as isolated pulmonary fibrosis. Our study expands the genetic
309 spectrum of this entity by describing three germline *RPA1* variants clustering to DBD-A to be associated
310 with a novel Mendelian disorder that clinically resembles a TBD/STS with short telomeres. Consistent
311 with the variable expressivity and penetrance observed in TBD/STS, the four affected individuals
312 developed a wide range of disease features at various ages with the common denominator of telomere
313 shortening. Constitutional manifestations included facial and eye anomalies present in two patients,
314 pulmonary disease in two, and a classic mucocutaneous triad in one. Hematopoietic system was
315 affected in three patients who had BMF, MDS, T- and B-cell lymphopenia and hypogammaglobulinemia.
316 Only one patient (P3) did not have abnormal blood counts, thereby not prompting further marrow
317 analysis. Similar to other TBD/STS manifestations reported in literature³⁷, it is possible that this patient's
318 disease had slow progression in hematopoietic system while resulting in premature aging in the lungs
319 manifesting as pulmonary fibrosis.

320
321 The well-established role of RPA1 in telomere maintenance using mammalian and non-mammalian
322 model systems predated our discovery of germline *RPA1* mutations in patients with TBD/STS and short
323 telomeres. Historically, many *S. cerevisiae rfa1* (*RPA1* paralog) mutants demonstrated increased
324 sensitivity from DNA damage, defective checkpoints, and gross chromosomal aberrations owing to RPA1
325 function in DNA replication and repair^{18,19,38}. Smith et al. first showed the presence of RPA at the
326 telomeric ends maximally during S phase, as well as, telomere shortening in a synergistic *yku70-rfa1-*
327 *D228Y S. cerevisiae* model³⁸. *rfa1-D228Y* was then modeled in *S. pombe* (paralog is *rad11-D223Y*), which
328 confirmed sensitivity to UV and γ -irradiation and exhibited reduced telomere length, suggesting that
329 RPA is directly involved in telomere maintenance³². Follow up studies further supported the role of RPA1
330 in telomere biology by demonstrating RPA1 ability to bind and unfold telomeric G-quadruplexes^{26,28,39},
331 regulate telomerase and telomerase access to chromosomal ends^{24,40} and preventing accumulation of
332 single strand telomeric DNA in alternative lengthening of telomeres (ALT) positive cells²⁹. Furthermore,
333 *rad11-D223Y* in *S. pombe*, corresponding to human *RPA1* D228Y, was shown to reduce binding affinity
334 for telomeric ssDNA and G4 quadruplexes, resulting in telomere shortening²⁵⁻²⁷. Overall, multiple studies
335 have established the role of RPA1 in telomere biology.

336

337 Unlike the previously studied variants, all patient RPA1 mutant proteins exhibit enhanced binding to
338 ssDNA. Furthermore, *RPA1*^{V227A} and *RPA1*^{E240K} harbor increased binding affinity to telomeric sequences
339 and a greater rate and extent of melting of G-quadruplexes whereas *RPA1*^{T270A} mutant was equivocal to
340 *RPA1*^{WT}. Binding of RPA to DNA is dynamic and regulates loading of other essential proteins on ssDNA. It
341 is plausible that GOF *RPA1*^{V227A} and *RPA1*^{E240K} mutations alter the access between chromosomal ends
342 and telomere maintenance machinery such as shelterin or telomerase complex and/or challenge the
343 RPA-to-POT1 switch and POT1 capping function, ultimately leaving telomeric ends vulnerable to
344 telomere degrading transactions⁴¹. Additionally, specific point mutations might affect interactions of
345 RPA1 with other proteins, which could explain why *RPA1*^{T270A} behaves different than other RPA1
346 mutants in binding to telomere sequences. The molecular mechanism by which RPA1 exerts telomere
347 maintenance is highly complex and remains elusive, requiring further investigation.

348

349 To directly examine whether a single amino acid exchange in RPA1 can be deleterious to eukaryotic
350 cells, we modeled *RPA1*^{E240K} variant in an iPSC model derived from a healthy donor. We deliberately
351 chose to introduce patient *RPA1*^{E240K} mutation into a healthy donor iPSC cell line instead of generating
352 patient derived iPSCs to eliminate the confounding effect of other unknown patient-specific mutations.
353 The rationale for establishing a homozygous knock-in was to avoid the development of rescue events
354 found in P1 and to exaggerate the biological phenotype for a gene variant that is associated with a late-
355 onset disease. We were able to recapitulate the biological phenotype of significant telomere shortening
356 in *RPA1*^{E240K} iPSC, as well as iPSC-derived hematopoiesis. Finally, we demonstrated that *RPA1*^{E240K}
357 mutation resulted in reduced capacity to generate iPSC-derived HP and decreased erythroid/myeloid
358 differentiation. This is in line with other reported iPSC short telomere disease models where
359 hematopoietic insufficiency has been observed⁴².

360

361 Stereotypic dyskeratosis congenita shows a progressive course with BMF leading to severe cytopenias
362 over time⁶. Remarkably, over 18 years, P1 followed an atypical course for TBD/STS marked by
363 stabilization of hematological features. Using this thread, we unraveled the unique propensity of
364 germline *RPA1*^{E240K} mutation to facilitate the development of two independent somatic genetic escape
365 lesions in P1. These were a second-site truncating *RPA1* mutation causing degradation of germline
366 mutant RNA and a UPD17p recombination resulting in replacement of germline variant with a wild type
367 allele. It seems that these mosaic events can expand and outcompete the native state *RPA1*-mutated
368 hematopoiesis without signs of exhaustion or malignant transformation. Somatic genetic rescue in

369 hematopoiesis has been described in TBD/STS genes such as *TERC*, *TERT*, *TINF2*, and *DKC1*, which arise in
370 response to LOF mutations⁴³⁻⁴⁸. The novelty of our finding lies in the identification of somatic rescue
371 arising in response to a GOF *RPA1*^{E240K} mutation, a known phenomenon recently described in patients
372 with GOF mutations in *SAMD9/SAMD9L* genes⁴⁹⁻⁵¹. Additionally, we observed improvement of oral
373 leukoplakia in P1 over time. One can speculate that mucosal tissue in this patient also underwent
374 somatic reversion, given that somatic mosaicism has been recently shown to be common in healthy
375 human tissues⁵².

376
377 Our study does have potential limitations that should be noted. Firstly, due to the small size of our
378 cohort, we are unable to characterize the full phenotypic spectrum associated with *RPA1* mutations.
379 Secondly, telomere length was measured either by flow-FISH or TRF Southern blot, which was inherent
380 to our patient cohort, presenting in four countries at different ages to unique providers with different
381 strategies for sample banking. Although outside the scope of this study, further research efforts are
382 required to understand the exact mechanism of how *RPA1* mutations cause telomere shortening, how
383 *RPA* regulates telomere length, and how this compares to other telomere associated genes^{53,54}.

384
385 In summary, we identify *RPA1* mutations to be associated with telomere shortening in humans, which
386 calls for careful consideration of *RPA1* missense variants in the workup of patients with TBD/STS
387 phenotypes. Germline *RPA1* variants can either be permissive, as seen with *RPA1*^{V227A} that is associated
388 with reduced penetrance or severely “hematotoxic” leading to somatic inactivation, as observed with
389 *RPA1*^{E240K}. We speculate that germline *RPA1* alterations may be more common in human disease, given
390 that somatic *RPA1* mutations occur in ~1% of cancers⁵⁵. Additional efforts are needed to not only find
391 further pathogenic *RPA1* variants but to also elucidate the role of *RPA1* in human telomere biology.

392 **ACKNOWLEDGEMENTS**

393 This work was supported by grants from the ERAPERMED GATA2-HuMo 2018-123, Deutsche Krebshilfe
394 Max Eder Grant 109005, Fritz-Thyssen Foundation 10.17.1.026MN, and St Jude American Lebanese
395 Syrian Associated Charities (ALSAC) (to MWW), José Carreras Leukämie-Stiftung (to VPL), BMBF MyPred
396 01GM1911A (to CMN, MWW, ME). Research reported in this manuscript was supported by the NIH
397 Common Fund, through the Office of Strategic Coordination/Office of the NIH Director under Award
398 Number U01HG007709. The content is solely the responsibility of the authors and does not necessarily
399 represent the official views of the National Institutes of Health. The St. Jude Cancer Center Core
400 Cytogenetics laboratory is supported by NIH, NCI (P30 CA21765-41) and ALSAC. MS is supported by
401 R35GM131704 and P30CA086862SC. PR, CS, and CK are supported by the Agence Nationale de la
402 Recherche (ANR-20-CE12-0012TeloRPA). HB and AK are supported by Deutsche Forschungsgemeinschaft
403 (DFG, German Research Foundation) under Germany's Excellence Strategy (EXC 22167-390884018). P3
404 exome study was supported by a grant from the Chancellerie des Universités de Paris (legs Poix). VG and
405 PR laboratories are supported by the "Ligue Nationale Contre le Cancer" (LNCC) (Equipe labélisée). PR is
406 a scientist from Centre National de la Recherche Scientifique (CNRS). SC is supported by Project
407 Fondation ARC, Projet Emergence-Cancéropôle PACA. We thank the patients for participation and
408 acknowledge our collaborators: Dirk Lebrecht, Marco Teller, Ali-Riza Kaya Wilfried Truckenmüller, Maria
409 Siskou-Zwecker, Axel Gebert (Freiburg) for laboratory assistance and data management; Loizos Petrikos
410 and Kondylia Antoniadis (Athens) for patient management; Ibrahima Ba, Bruno Crestani (Marseille Cancer
411 Research Centre) for technical assistance; Dr. Lindsay Burrage for exome analysis and Dr. Filiz Seeborg
412 for P4 referral; Yawei Hui, Shibiao Wan, Yiping Fan, Gang Wu (St Jude Center for Applied Bioinformatics),
413 OMICS computing cluster (University of Lübeck, Germany), Emmanuelle Olivier and Patrick Nitschké
414 (Imagine Institute, Paris, France/ Université de Paris) for bioinformatics support; Robert Durruthy-
415 Durruthy (MissionBio) for support on scDNAseq analysis; Amabel Orogo (Illumina) and Jordan Sheetz
416 (Bio-Rad Laboratories) for technical support; Dr. Mihaela Onciu (St Jude Department of Pathology) for
417 iPSC derived erythroid and myeloid cytology review; Dr. Aaron Taylor from St Jude Center of Imaging for
418 imaging consultation; Drs. Sunita Dsouza, Maria Lillo Osuna and Min-Joon Han (St. Jude) for iPSC
419 technical assistance; Virginia Valentine, and Julia Wilbourne (St Jude Cytogenetics core); and Drs.
420 Mitchell Weiss and John Crispino for helpful discussions.

421 **AUTHORSHIP CONTRIBUTION**

422 RS, SSS, MWW, CS, SC, MSW, MS conceived and designed the experiments. RS, SSS, AK, HB, TCC, MB,
423 VPL, JAR, CK, MWW performed genomic data analysis. RS, MH, SLG, CG, LS, FB, MBV, SMPM, AGF, DC,
424 VG, CS, PR, MSW, MS, and SC performed and/or interpreted functional experiments. FB, SH, ML, CK, MC,
425 SN, JAR, SP, CMN, ME, RS, MWW were involved in patient care, collecting clinical data and clinical
426 testing. MWW, SC, MSW, MS supervised the experiments, and MWW oversaw study design. All authors
427 contributed to the manuscript and approved of the final version.

428

429 **COMPETING INTERESTS STATEMENT**

430 The Department of Molecular and Human Genetics at Baylor College of Medicine receives revenue from
431 clinical genetic testing completed at Baylor Genetics Laboratories.

432

433 Appendix: study group members

434

435 The members of the Undiagnosed Diseases Network are the following:

436

437 Maria T. Acosta, Margaret Adam, David R. Adams, Pankaj B. Agrawal, Justin Alvey, Laura
 438 Amendola, Ashley Andrews, Euan A. Ashley, Mahshid S. Azamian, Carlos A. Bacino, Guney
 439 Bademci, Eva Baker, Ashok Balasubramanyam, Dustin Baldrige, Jim Bale, Michael Bamshad,
 440 Deborah Barbooth, Pinar Bayrak-Toydemir, Anita Beck, Alan H. Beggs, Edward Behrens, Gill
 441 Bejerano, Jimmy Bennet, Beverly Berg-Rood, Jonathan A. Bernstein, Gerard T. Berry, Anna
 442 Bican, Stephanie Bivona, Elizabeth Blue, John Bohnsack, Carsten Bonnenmann, Devon
 443 Bonner, Lorenzo Botto, Brenna Boyd, Lauren C. Briere, Elly Brokamp, Gabrielle Brown,
 444 Elizabeth A. Burke, Lindsay C. Burrage, Manish J. Butte, Peter Byers, William E. Byrd, John
 445 Carey, Olveen Carrasquillo, Ta Chen Peter Chang, Sirisak Chanprasert, Hsiao-Tuan Chao,
 446 Gary D. Clark, Terra R. Coakley, Laurel A. Cobban, Joy D. Cogan, Matthew Coggins, F.
 447 Sessions Cole, Heather A. Colley, Cynthia M. Cooper, Heidi Cope, William J. Craigen, Andrew
 448 B. Crouse, Michael Cunningham, Precilla D'Souza, Hongzheng Dai, Surendra Dasari, Joie
 449 Davis, Jyoti G. Dayal, Matthew Dearnorff, Esteban C. Dell'Angelica, Katrina Dipple, Daniel
 450 Doherty, Naghmeh Dorrani, Argenia L. Doss, Emilie D. Douine, David D. Draper, Laura Duncan,
 451 Dawn Earl, David J. Eckstein, Lisa T. Emrick, Christine M. Eng, Cecilia Esteves, Marni Falk,
 452 Liliana Fernandez, Carlos Ferreira, Elizabeth L. Fieg, Laurie C. Findley, Paul G. Fisher, Brent L.
 453 Fogel, Irman Forghani, William A. Gahl, Ian Glass, Bernadette Gochuico, Rena A. Godfrey,
 454 Katie Golden-Grant, Madison P. Goldrich, David B. Goldstein, Alana Grajewski, Catherine A.
 455 Groden, Irma Gutierrez, Sihoun Hahn, Rizwan Hamid, Kelly Hassey, Nichole Hayes, Frances
 456 High, Anne Hing, Fuki M. Hisama, Ingrid A. Holm, Jason Hom, Martha Horike-Pyne, Alden
 457 Huang, Yong Huang, Laryssa Huryn, Rosario Isasi, Fariha Jamal, Gail P. Jarvik, Jeffrey Jarvik,
 458 Suman Jayadev, Lefkothea Karaviti, Jennifer Kennedy, Shamika Ketkar, Dana Kiley, Shilpa N.
 459 Kobren, Isaac S. Kohane, Jennefer N. Kohler, Deborah Krakow, Donna M. Krasnewich, Elijah
 460 Kravets, Susan Korrick, Mary Koziura, Joel B. Krier, Seema R. Lalani, Byron Lam, Christina
 461 Lam, Grace L. LaMoure, Brendan C. Lanpher, Ian R. Lanza, Lea Latham, Kimberly LeBlanc,
 462 Brendan H. Lee, Hane Lee, Roy Levitt, Richard A. Lewis, Sharyn A. Lincoln, Pengfei Liu, Xue
 463 Zhong Liu, Nicola Longo, Sandra K. Loo, Joseph Loscalzo, Richard L. Maas, John MacDowall,
 464 Ellen F. Macnamara, Calum A. MacRae, Valerie V. Maduro, Bryan C. Mak, May Christine V.
 465 Malicdan, Laura A. Mamounas, Teri A. Manolio, Rong Mao, Kenneth Maravilla, Thomas C.
 466 Markello, Ronit Marom, Gabor Marth, Beth A. Martin, Martin G. Martin, Julian A. Martínez-
 467 Agosto, Shruti Marwaha, Jacob McCauley, Allyn McConkie-Rosell, Alexa T. McCray, Elisabeth
 468 McGee, Heather Mefford, J. Lawrence Merritt, Matthew Might, Ghayda Mirzaa, Eva Morava,
 469 Paolo M. Moretti, Deborah Mosbrook-Davis, John J. Mulvihill, Mariko Nakano-Okuno, Avi Nath,
 470 Stan F. Nelson, John H. Newman, Sarah K. Nicholas, Deborah Nickerson, Shirley Nieves-
 471 Rodriguez, Donna Novacic, Devin Oglesbee, James P. Orenge, Laura Pace, Stephen Pak, J.
 472 Carl Pallais, Christina GS. Palmer, Jeanette C. Papp, Neil H. Parker, John A. Phillips III,
 473 Jennifer E. Posey, Lorraine Potocki, Bradley Power, Barbara N. Pusey, Aaron Quinlan, Wendy
 474 Raskind, Archana N. Raja, Deepak A. Rao, Genecee Renteria, Chloe M. Reuter, Lynette Rives,
 475 Amy K. Robertson, Lance H. Rodan, Jill A. Rosenfeld, Natalie Rosenwasser, Francis Rossignol,
 476 Maura Ruzhnikov, Ralph Sacco, Jacinda B. Sampson, Mario Saporta, C. Ron Scott, Judy
 477 Schaechter, Timothy Schedl, Kelly Schoch, Daryl A. Scott, Vandana Shashi, Jimann Shin,
 478 Rebecca Signer, Edwin K. Silverman, Janet S. Sinsheimer, Kathy Sisco, Edward C. Smith,
 479 Kevin S. Smith, Emily Solem, Lilianna Solnica-Krezel, Ben Solomon, Rebecca C. Spillmann,
 480 Joan M. Stoler, Jennifer A. Sullivan, Kathleen Sullivan, Angela Sun, Shirley Sutton, David A.
 481 Sweetser, Virginia Sybert, Holly K. Tabor, Amelia L. M. Tan, Queenie K.-G. Tan, Mustafa Tekin,
 482 Fred Telischi, Willa Thorson, Audrey Thurm, Cynthia J. Tifft, Camilo Toro, Alyssa A. Tran,
 483 Brianna M. Tucker, Tiina K. Urv, Adeline Vanderver, Matt Velinder, Dave Viskochil, Tiphane P.
 484 Vogel, Colleen E. Wahl, Stephanie Wallace, Nicole M. Walley, Chris A. Walsh, Melissa Walker,
 485 Jennifer Wambach, Jijun Wan, Lee-kai Wang, Michael F. Wangler, Patricia A. Ward, Daniel

486 Wegner, Monika Weisz-Hubshman, Mark Wener, Tara Wenger, Katherine Wesseling Perry,
487 Monte Westerfield, Matthew T. Wheeler, Jordan Whitlock, Lynne A. Wolfe, Jeremy D. Woods,
488 Kim Worley, Shinya Yamamoto, John Yang, Muhammad Yousef, Diane B. Zastrow, Wadih Zein,
489 Chunli Zhao, Stephan Zuchner, Hugo Bellen, and Rachel Mahoney.
490
491

492 **REFERENCES**

- 493 1. Blackburn EH, Epel ES, Lin J. Human telomere biology: A contributory and interactive factor in
494 aging, disease risks, and protection. *Science*. 2015;350(6265):1193-1198.
- 495 2. Niewisch MR, Savage SA. An update on the biology and management of dyskeratosis congenita
496 and related telomere biology disorders. *Expert Rev Hematol*. 2019;12(12):1037-1052.
- 497 3. Schratz KE, Haley L, Danoff SK, et al. Cancer spectrum and outcomes in the Mendelian short
498 telomere syndromes. *Blood*. 2020;135(22):1946-1956.
- 499 4. Calado RT, Young NS. Telomere diseases. *N Engl J Med*. 2009;361(24):2353-2365.
- 500 5. Dokal I, Vulliamy T, Mason P, Bessler M. Clinical utility gene card for: Dyskeratosis congenita -
501 update 2015. *Eur J Hum Genet*. 2015;23(4).
- 502 6. Savage SA. Dyskeratosis Congenita. In: Adam MP, Ardinger HH, Pagon RA, et al., eds.
503 *GeneReviews((R))*. Seattle (WA)1993.
- 504 7. Wold MS. Replication protein A: a heterotrimeric, single-stranded DNA-binding protein required
505 for eukaryotic DNA metabolism. *Annu Rev Biochem*. 1997;66:61-92.
- 506 8. Bhat KP, Cortez D. RPA and RAD51: fork reversal, fork protection, and genome stability. *Nat*
507 *Struct Mol Biol*. 2018;25(6):446-453.
- 508 9. de Laat WL, Appeldoorn E, Sugawara K, Weterings E, Jaspers NG, Hoeijmakers JH. DNA-binding
509 polarity of human replication protein A positions nucleases in nucleotide excision repair. *Genes*
510 *Dev*. 1998;12(16):2598-2609.
- 511 10. Krejci L, Altmannova V, Spirek M, Zhao X. Homologous recombination and its regulation. *Nucleic*
512 *Acids Res*. 2012;40(13):5795-5818.
- 513 11. Li GM. Mechanisms and functions of DNA mismatch repair. *Cell Res*. 2008;18(1):85-98.
- 514 12. Caldwell CC, Spies M. Dynamic elements of replication protein A at the crossroads of DNA
515 replication, recombination, and repair. *Crit Rev Biochem Mol Biol*. 2020;55(5):482-507.
- 516 13. Chen R, Wold MS. Replication protein A: single-stranded DNA's first responder: dynamic DNA-
517 interactions allow replication protein A to direct single-strand DNA intermediates into different
518 pathways for synthesis or repair. *Bioessays*. 2014;36(12):1156-1161.
- 519 14. Dahai Y, Sanyuan S, Hong L, Di Z, Chong Z. A relationship between replication protein A and
520 occurrence and prognosis of esophageal carcinoma. *Cell Biochem Biophys*. 2013;67(1):175-180.
- 521 15. Givalos N, Gakiopoulou H, Skliri M, et al. Replication protein A is an independent prognostic
522 indicator with potential therapeutic implications in colon cancer. *Mod Pathol*. 2007;20(2):159-
523 166.
- 524 16. Wang J, Yang T, Chen H, Li H, Zheng S. Oncogene RPA1 promotes proliferation of hepatocellular
525 carcinoma via CDK4/Cyclin-D pathway. *Biochem Biophys Res Commun*. 2018;498(3):424-430.
- 526 17. Zhu Y, Yi Y, Bai B, et al. The silencing of replication protein A1 induced cell apoptosis via
527 regulating Caspase 3. *Life Sci*. 2018;201:141-149.
- 528 18. Chen C, Kolodner RD. Gross chromosomal rearrangements in *Saccharomyces cerevisiae*
529 replication and recombination defective mutants. *Nat Genet*. 1999;23(1):81-85.
- 530 19. Chen C, Umezu K, Kolodner RD. Chromosomal rearrangements occur in *S. cerevisiae* rfa1
531 mutator mutants due to mutagenic lesions processed by double-strand-break repair. *Mol Cell*.
532 1998;2(1):9-22.
- 533 20. Haring SJ, Mason AC, Binz SK, Wold MS. Cellular functions of human RPA1. Multiple roles of
534 domains in replication, repair, and checkpoints. *J Biol Chem*. 2008;283(27):19095-19111.
- 535 21. Wang Y, Putnam CD, Kane MF, et al. Mutation in Rpa1 results in defective DNA double-strand
536 break repair, chromosomal instability and cancer in mice. *Nat Genet*. 2005;37(7):750-755.
- 537 22. Wang Y, Zhang W, Edelman L, Kolodner RD, Kucherlapati R, Edelman W. Cis lethal genetic
538 interactions attenuate and alter p53 tumorigenesis. *Proc Natl Acad Sci U S A*.
539 2010;107(12):5511-5515.

- 540 23. Smith J, Rothstein R. A mutation in the gene encoding the *Saccharomyces cerevisiae* single-
541 stranded DNA-binding protein Rfa1 stimulates a RAD52-independent pathway for direct-repeat
542 recombination. *Mol Cell Biol*. 1995;15(3):1632-1641.
- 543 24. Luciano P, Coulon S, Faure V, et al. RPA facilitates telomerase activity at chromosome ends in
544 budding and fission yeasts. *EMBO J*. 2012;31(8):2034-2046.
- 545 25. Audry J, Maestroni L, Delagoutte E, et al. RPA prevents G-rich structure formation at lagging-
546 strand telomeres to allow maintenance of chromosome ends. *EMBO J*. 2015;34(14):1942-1958.
- 547 26. Ray S, Qureshi MH, Malcolm DW, Budhathoki JB, Celik U, Balci H. RPA-mediated unfolding of
548 systematically varying G-quadruplex structures. *Biophys J*. 2013;104(10):2235-2245.
- 549 27. Safa L, Delagoutte E, Petrusseva I, et al. Binding polarity of RPA to telomeric sequences and
550 influence of G-quadruplex stability. *Biochimie*. 2014;103:80-88.
- 551 28. Salas TR, Petrusseva I, Lavrik O, et al. Human replication protein A unfolds telomeric G-
552 quadruplexes. *Nucleic Acids Res*. 2006;34(17):4857-4865.
- 553 29. Grudic A, Jul-Larsen A, Haring SJ, et al. Replication protein A prevents accumulation of single-
554 stranded telomeric DNA in cells that use alternative lengthening of telomeres. *Nucleic Acids Res*.
555 2007;35(21):7267-7278.
- 556 30. Kibe T, Ono Y, Sato K, Ueno M. Fission yeast Taz1 and RPA are synergistically required to prevent
557 rapid telomere loss. *Mol Biol Cell*. 2007;18(6):2378-2387.
- 558 31. Kobayashi Y, Sato K, Kibe T, et al. Expression of mutant RPA in human cancer cells causes
559 telomere shortening. *Biosci Biotechnol Biochem*. 2010;74(2):382-385.
- 560 32. Ono Y, Tomita K, Matsuura A, et al. A novel allele of fission yeast rad11 that causes defects in
561 DNA repair and telomere length regulation. *Nucleic Acids Res*. 2003;31(24):7141-7149.
- 562 33. Yang Y, Muzny DM, Xia F, et al. Molecular findings among patients referred for clinical whole-
563 exome sequencing. *JAMA*. 2014;312(18):1870-1879.
- 564 34. Sahoo SS, Pastor VB, Goodings C, et al. Clinical evolution, genetic landscape and trajectories of
565 clonal hematopoiesis in SAMD9/SAMD9L syndromes. *Nat Med*. 2021.
- 566 35. Werner B, Beier F, Hummel S, et al. Reconstructing the in vivo dynamics of hematopoietic stem
567 cells from telomere length distributions. *Elife*. 2015;4.
- 568 36. Heiss NS, Knight SW, Vulliamy TJ, et al. X-linked dyskeratosis congenita is caused by mutations in
569 a highly conserved gene with putative nucleolar functions. *Nat Genet*. 1998;19(1):32-38.
- 570 37. Kam MLW, Nguyen TTT, Ngeow JYY. Telomere biology disorders. *NPJ Genom Med*. 2021;6(1):36.
- 571 38. Smith J, Zou H, Rothstein R. Characterization of genetic interactions with RFA1: the role of RPA
572 in DNA replication and telomere maintenance. *Biochimie*. 2000;82(1):71-78.
- 573 39. Cohen S, Jacob E, Manor H. Effects of single-stranded DNA binding proteins on primer extension
574 by telomerase. *Biochim Biophys Acta*. 2004;1679(2):129-140.
- 575 40. Schramke V, Luciano P, Brevet V, et al. RPA regulates telomerase action by providing Est1p
576 access to chromosome ends. *Nat Genet*. 2004;36(1):46-54.
- 577 41. Flynn RL, Centore RC, O'Sullivan RJ, et al. TERRA and hnRNPA1 orchestrate an RPA-to-POT1
578 switch on telomeric single-stranded DNA. *Nature*. 2011;471(7339):532-536.
- 579 42. Winkler T, Hong SG, Decker JE, et al. Defective telomere elongation and hematopoiesis from
580 telomerase-mutant aplastic anemia iPSCs. *J Clin Invest*. 2013;123(5):1952-1963.
- 581 43. Alder JK, Stanley SE, Wagner CL, Hamilton M, Hanumanthu VS, Armanios M. Exome sequencing
582 identifies mutant TINF2 in a family with pulmonary fibrosis. *Chest*. 2015;147(5):1361-1368.
- 583 44. Gutierrez-Rodriguez F, Donaires FS, Pinto A, et al. Pathogenic TERT promoter variants in
584 telomere diseases. *Genet Med*. 2019;21(7):1594-1602.
- 585 45. Jongmans MC, Verwiel ET, Heijdra Y, et al. Revertant somatic mosaicism by mitotic
586 recombination in dyskeratosis congenita. *Am J Hum Genet*. 2012;90(3):426-433.
- 587 46. Maryoung L, Yue Y, Young A, et al. Somatic mutations in telomerase promoter counterbalance
588 germline loss-of-function mutations. *J Clin Invest*. 2017;127(3):982-986.

- 589 47. Perdignes N, Perin JC, Schiano I, et al. Clonal hematopoiesis in patients with dyskeratosis
590 congenita. *Am J Hematol*. 2016;91(12):1227-1233.
- 591 48. Revy P, Kannengiesser C, Fischer A. Somatic genetic rescue in Mendelian haematopoietic
592 diseases. *Nat Rev Genet*. 2019;20(10):582-598.
- 593 49. Buonocore F, Kuhnen P, Suntharalingham JP, et al. Somatic mutations and progressive
594 monosomy modify SAMD9-related phenotypes in humans. *J Clin Invest*. 2017;127(5):1700-1713.
- 595 50. Chen DH, Below JE, Shimamura A, et al. Ataxia-Pancytopenia Syndrome Is Caused by Missense
596 Mutations in SAMD9L. *Am J Hum Genet*. 2016;98(6):1146-1158.
- 597 51. Narumi S, Amano N, Ishii T, et al. SAMD9 mutations cause a novel multisystem disorder, MIRAGE
598 syndrome, and are associated with loss of chromosome 7. *Nat Genet*. 2016;48(7):792-797.
- 599 52. Yizhak K, Aguet F, Kim J, et al. RNA sequence analysis reveals macroscopic somatic clonal
600 expansion across normal tissues. *Science*. 2019;364(6444).
- 601 53. Fok WC, Shukla S, Vessoni AT, et al. Posttranscriptional modulation of TERC by PAPD5 inhibition
602 rescues hematopoietic development in dyskeratosis congenita. *Blood*. 2019;133(12):1308-1312.
- 603 54. Shukla S, Jeong HC, Sturgeon CM, Parker R, Batista LFZ. Chemical inhibition of PAPD5/7 rescues
604 telomerase function and hematopoiesis in dyskeratosis congenita. *Blood Adv*. 2020;4(12):2717-
605 2722.
- 606 55. Tate JG, Bamford S, Jubb HC, et al. COSMIC: the Catalogue Of Somatic Mutations In Cancer.
607 *Nucleic Acids Res*. 2019;47(D1):D941-D947.
608

609 TABLES
 610
 611

Patient features			Germline mutation					Disease features		
Patient	Gender	Age of onset (years)	<i>RPA1</i> status	Exon	VAF% (TD)	Population databases	CADD	Hematopoietic	Other	Recent status
P1	F	10	c.718G>A, p.E240K <i>de novo</i>	9	24%# (58)	absent	23.3	Refractory cytopenia of childhood	Mucocutaneous triad Congenital eye anomaly*	No interventions Stable blood counts at age 28 years
P2	F	13	c.680T>C, p.V227A	8	51% (118)	gnomADv3.1: 76078 genomes (1/152156 alleles)	26.9	Myelodysplastic syndrome with excess blasts	Mild restrictive lung disease Facial dysmorphism**	HSCT Death at age 14 years (GVHD, infection, pulmonary fibrosis)
P3	F	58			53% (49)	TOPMed freeze 8: 132345 genomes (2/264690 alleles)		BM not examined CBC normal	Familial pulmonary fibrosis***	Progression of pulmonary fibrosis on antifibrotics
P4	F	birth	c.808A>G, p.T270A <i>de novo</i>	10	41% (51)	absent	20.9	BM not examined Low TRECs Lymphopenia Hypogammaglobulinemia	Prematurity (33 weeks)	IgG replacement Stable CBC at age 3 years

612
 613 **Table 1: Genomic and clinical features of patients with germline heterozygous *RPA1* variants.** F, female; TD, total depth; gnomAD v3.1 and TOPMed
 614 Bravo freeze 8 population databases with population genome sequencing data; CADD, combined annotation dependent depletion, pathogenicity
 615 threshold of 15; DANN, deleterious annotation of genetic variants using neural networks, range of 0 to 1 with higher values with greater probability of
 616 being damaging; BM, bone marrow; CBC, complete blood count; TRECs, T-cell receptor excision circles; HSCT, hematopoietic stem cell transplantation;
 617 GVHD, graft versus host disease.
 618 # Confirmed germline in fibroblasts, decreased VAF is due to UPD in blood cells; *Congenital persistent hyperplastic primary vitreous of the left eye
 619 requiring enucleation; **Bilateral blepharophimosis, epicanthus inversus, eyelid ptosis, and thick eyebrows with high arch found in P2 and carrier father;
 620 *** Pulmonary fibrosis diagnosed in two sisters of P3 (Supplemental Fig. 2). NM_002945.5 was used for variant nomenclature.

621 **FIGURE LEGENDS**

622 **Figure 1. Clinical characteristics of patients with identified *RPA1* variants.** (A) Germline *RPA1* variants
 623 identified in four pedigrees using exome sequencing. Black filled, open dotted and open symbols denote
 624 affected individuals with heterozygous (het) *RPA1* mutations, unaffected carriers, and unaffected family
 625 members without mutations, respectively. (B) Top panel: Schematic of the *RPA1* gene with 17 coding
 626 exons illustrated as black lines and untranslated regions shown in red (NM_002945.5). The three unique
 627 patient variants are located on exons 8, 9 and 10. Bottom panel: Human *RPA1* protein illustration with
 628 four oligonucleotide/oligosaccharide-binding (OB) fold domains F, A, B, and C with amino acid
 629 boundaries shown below. OB folds A, B and C are single strand (ss) DNA binding domains. Red arrows
 630 indicate location of 3 *RPA1* missense alterations. (C) Bone marrow (BM) findings in patient cohort (top
 631 panel): P1 BM aspirate smears (Wright-Giemsa staining) at time of clinical presentation at age 10 years
 632 showing marked reduction in cell content with hypoplasia of all lineages (left image) and megaloblastic
 633 maturation of erythroid precursors (middle image). P2 BM infiltrated with myeloblasts (right image)
 634 consistent with myelodysplastic syndrome with excess blasts. Pulmonary findings by chest computed
 635 tomography (CT) in patient cohort (middle panel): P2 chest CT (left image) during hospitalization
 636 demonstrating necrotizing pneumonitis with diffuse ground-glass opacities and large air-filled cavities
 637 with differential diagnosis including pulmonary GVHD, opportunistic infection(s), pulmonary fibrosis, or
 638 a combination of the above conditions. P3 presented at age 58 years with cough and exertional dyspnea
 639 with chest CT (middle image) findings showing intralobular reticulations with traction bronchiectasis and
 640 mild honeycombing, with left asymmetric and basal, subpleural predominance. At 61 years, P3 chest CT
 641 (right image) showed significant progression of asymmetric lung fibrosis with left predominance and
 642 massive basal honeycombing. Mucocutaneous abnormalities in P1 (bottom panel): oral leukoplakia at 19
 643 years of age (top left image) with mild improvement at 25 years of age (top right image), nail dystrophy
 644 (bottom left image) and reticular skin pigmentation on the ventral neck (bottom right image). (D)
 645 Telomere length analysis by flow cytometry-based-fluorescence in-situ hybridization (flow-FISH) was
 646 carried out in lymphocytes of P1 (red circles) and P4 (blue circles). P1 telomere length is less than 1st
 647 percentile at 24 and 27 years of age (red circles). P4 telomere length is at the 5th percentile at 1.75 years
 648 of age and less than 1st percentile at age 3.33 years (blue circles). All measurements were carried out in
 649 triplicates, and mean telomere length was calculated in kilobases (kb) in relation to the internal control
 650 (bovine thymocytes) with known telomere length. 356 healthy controls used for calculation of the 1st
 651 (solid line, bottom), 5th (dashed line, bottom), 95th (dashed line, top), and 99th (solid line, top) percentile
 652 curves. (E) Telomere restriction fragment (TRF) analysis in peripheral blood DNA from P2 and family and
 653 P3 compared to healthy age matched control (Ctrl), digested with *HinfI* and *RsaI* enzymes followed by
 654 separation on 0.7% agarose gel.

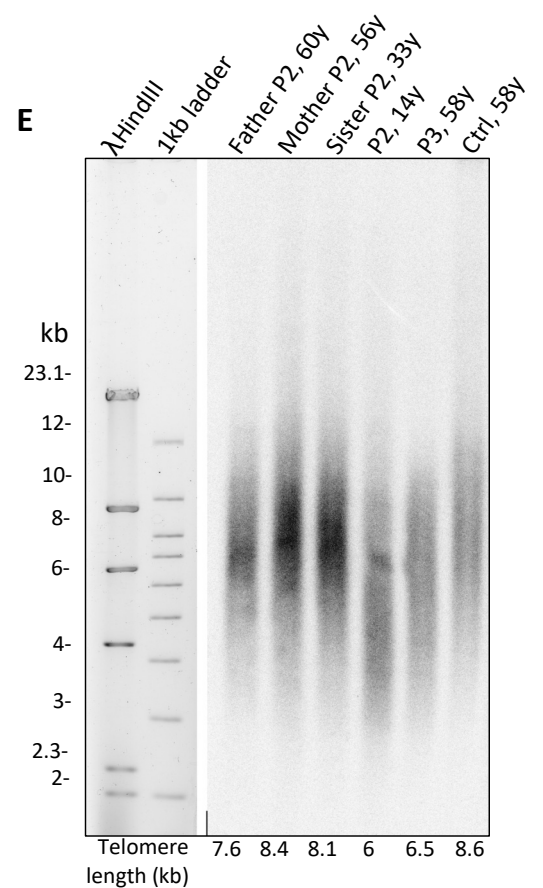
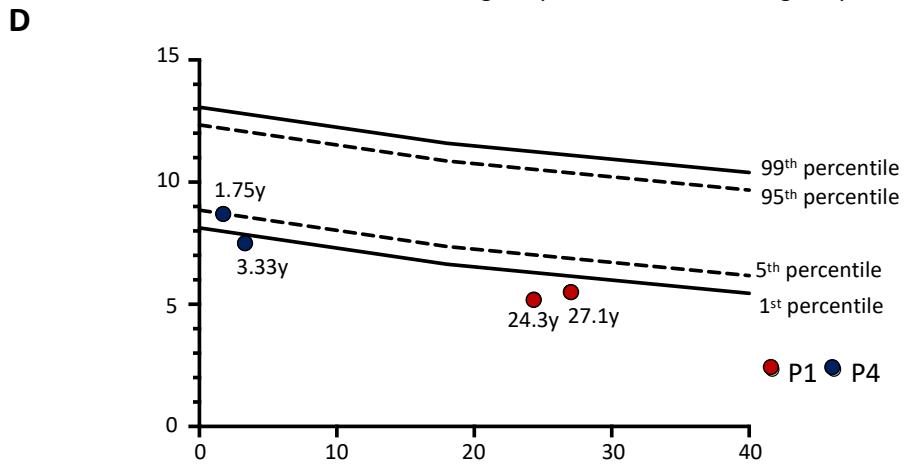
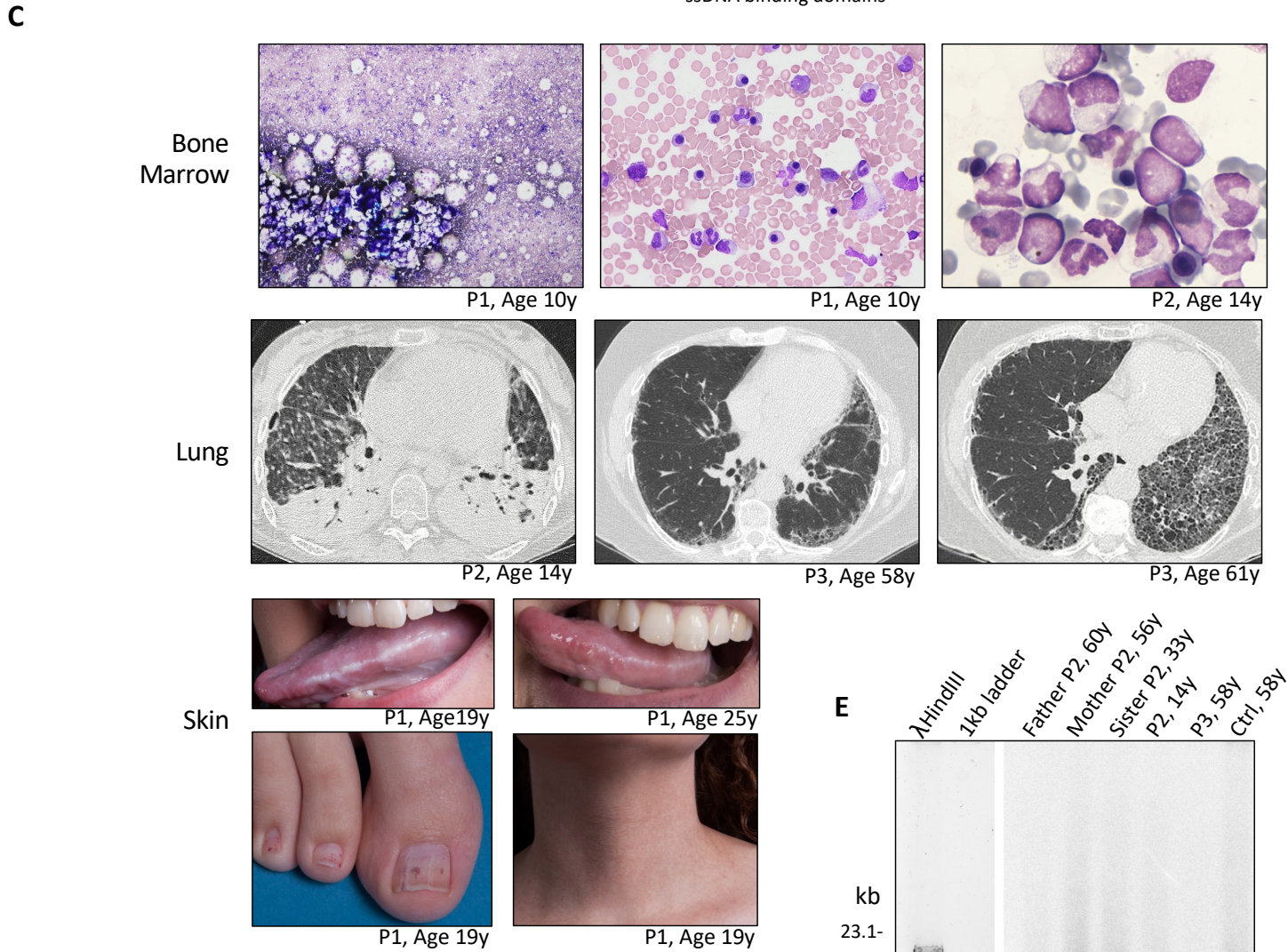
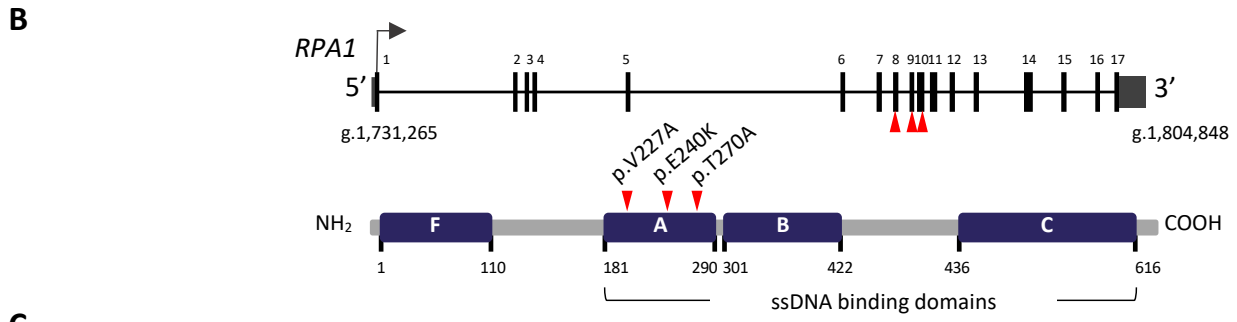
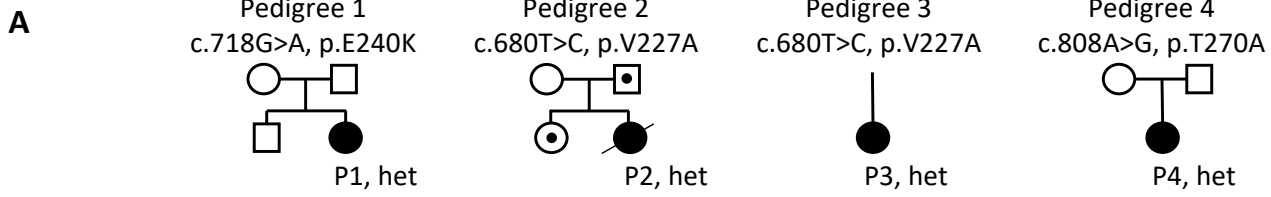
655
 656 **Figure 2. All *RPA* mutant heterotrimeric proteins exhibit increased affinity for ssDNA and *RPA*^{V227A} and
 657 *RPA*^{E240K} possess increased capacity to unfold telomeric G-quadruplex (h-telG4) DNA.** (A) Schematic
 658 depiction of the experimental schemes for the FRET-based assays. Binding of *RPA*:*RPA1*^{WT} (*RPA*^{WT}),
 659 *RPA*:*RPA1*^{V227A} (*RPA*^{V227A}), *RPA*:*RPA1*^{V270A} (*RPA*^{V270A}) and *RPA*:*RPA1*^{E240K} (*RPA*^{E240K}) proteins was monitored
 660 using 1 nM dT30 ssDNA molecules (top), 1 nM dT15 or TTAGGGTAAGGGTAA telomeric DNA sequence
 661 (middle) labeled with Cy3 and Cy5 fluorescent dyes at the 5' and 3' ends, respectively. High FRET
 662 corresponds to free ssDNA, while low FRET reflects *RPA* binding. Unfolding of the telomeric G-

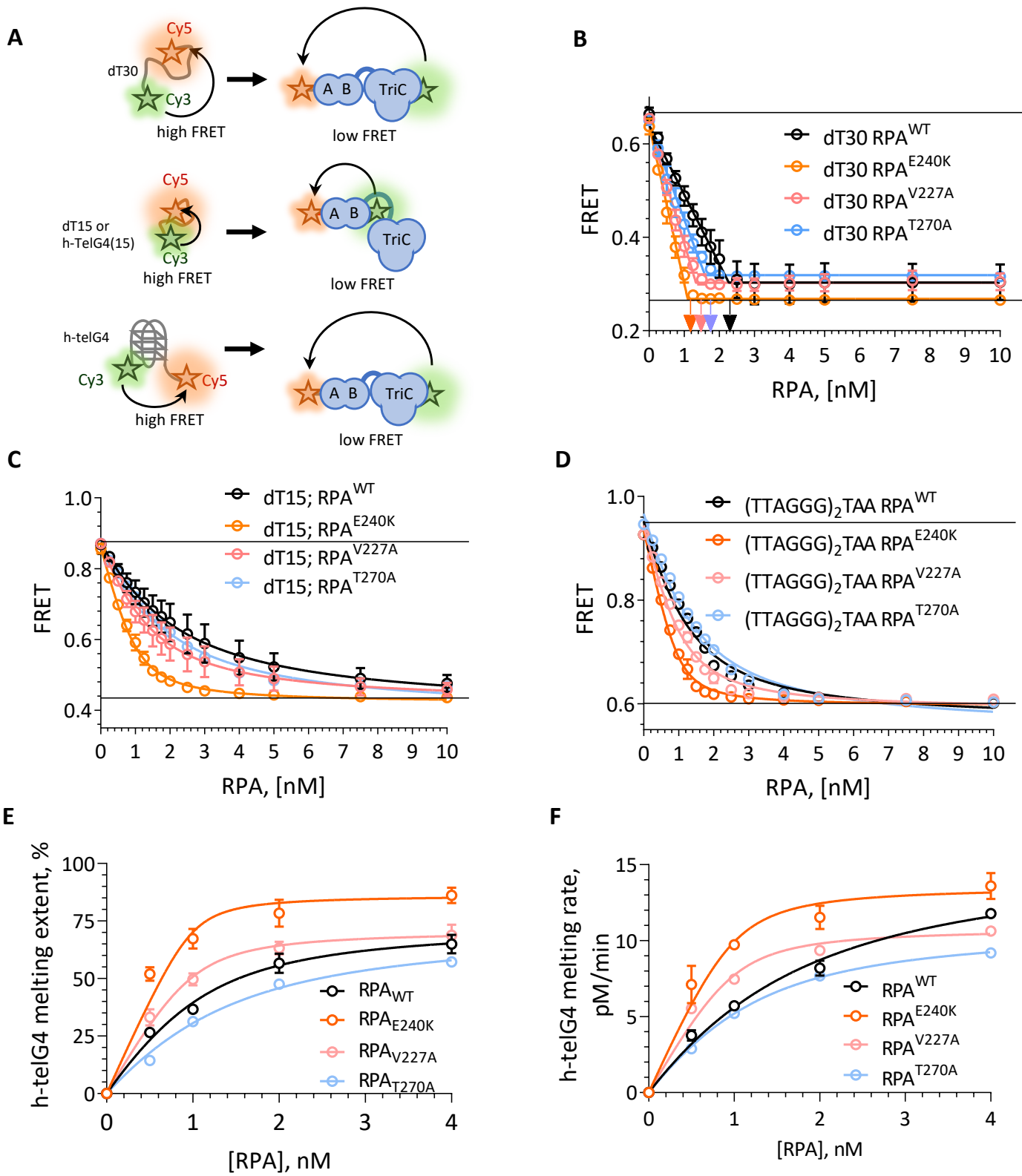
663 quadruplex (h-telG4) was monitored using (TTAGGG)₅ sequence. FRET between the Cy3 and Cy5 dyes
 664 calculated for the h-telG4 in the absence of proteins and in buffer containing K⁺ corresponds to 100%
 665 folded quadruplex, while the FRET value of h-telG4 in the presence of saturating concentrations of
 666 RPA^{E240K} in buffer containing Li⁺ corresponds to 100% unfolded h-telG4. (B) Stoichiometric binding (1
 667 RPA: 1 dT30 molecule) was observed for RPA^{E240K} (orange) and nearly stoichiometric binding was
 668 observed for the RPA^{WT} (black), RPA^{V227A} (pink) and RPA^{V270A} (blue). The arrows mark the respective
 669 protein concentrations at inflection points of the two-line linear regression fit. (C) dT15 and (D)
 670 TTAGGGTAAGGGTAA telomeric DNA sequence binding to RPA^{WT} (black), RPA^{V227A} (pink), RPA^{V270A} (blue)
 671 and RPA^{E240K} (orange). The data were fitted to quadratic binding equation. The calculated K_ds with
 672 respective fitting errors are listed in Supplemental Table 3. (E) and (F), Melting of the h-telG4 DNA,
 673 stabilized by the presence of 100 mM KCl. (E) Extents of the h-telG4 melting reactions were calculated
 674 from the plateaus of each respective time course. (F) h-telG4 melting rates for RPA^{WT} (black), RPA^{V227A}
 675 (pink), RPA^{V270A} (blue) and RPA^{E240K} (orange) were calculated from the slopes of FRET change during the
 676 first 20 seconds of each time course (Supplemental Fig. 4). The data were fitted to quadratic binding
 677 equation. The calculated apparent K_ds with respective fitting errors are listed in Supplemental Table 3. In
 678 all panels the data are shown as average for three independent experiments. Error bars represent
 679 standard deviation. Where not shown, error bars are smaller than the data points.

680
 681 **Figure 3. Human RPA1^{E240K} iPSC demonstrate telomere shortening and reduced hematopoietic**
 682 **potential.** (A) Left panel: Healthy control iPSC (RPA1^{WT}) following CRISPR/Cas9-guided homozygous
 683 c.718G>A (p.E240K, as E240K) modification within endogenous RPA1 locus (RPA1^{E240K}) confirmed with
 684 Sanger analysis. Right panel: Illustration of iPSC monolayer-based differentiation to hematopoietic
 685 progenitors and subsequently to erythroid and myeloid cell lineages. Day 10 HP cells were FACS-sorted
 686 and cultured in erythroid or myeloid differentiation media for 14 days. In parallel, iPSC-derived HP were
 687 further cultured until day 21 to assess for expression of pan-hematopoietic markers. (B) Immunoblot
 688 analysis of RPA1 expression in RPA1^{WT} and RPA1^{E240K} iPSC whole cell extracts with histone-H3 as loading
 689 control. (C) Telomere length in RPA1^{WT} passage 17 and RPA1^{E240K} passage 12 iPSCs (D) and iPSC-derived
 690 HP cells using quantitative fluorescence in situ hybridization (Q-FISH). Graphs represent mean ± SEM of
 691 one of three independent experiments (****P < 0.0001; Student t-test). (E) Decreased percentage of
 692 CD43⁺CD45⁺ RPA1^{E240K} hematopoietic cells compared to RPA1^{WT} at days 16 and 21. Data represent mean
 693 ± SEM of two independent experiments (*P = 0.03, **P = 0.0074; Student t-test). (F) Graphical
 694 representation of CD71⁺CD235⁺ erythroid cells from iPSC-derived erythroid cultures at day 14. Data
 695 represents mean ± SEM of 4 independent experiments (***P = 0.0002; Student t-test). I, Plot
 696 representation of CD45⁺CD11b⁺ myeloid cells from iPSC cultures. Data represent mean ± SEM of 2
 697 independent experiments (**P = 0.0018; Student t-test).

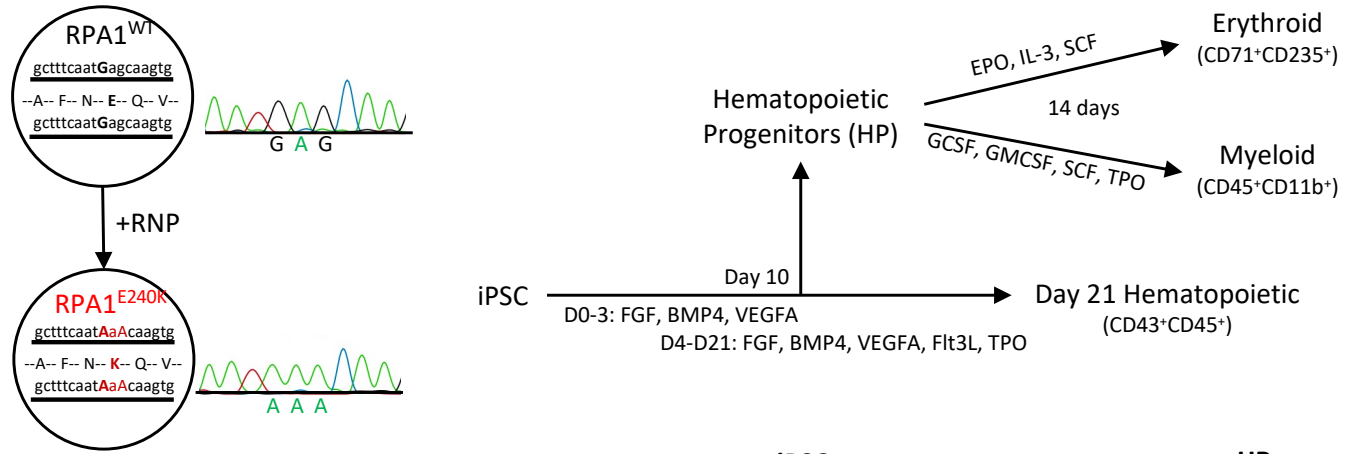
698
 699 **Figure 4. Natural evolution of disease and somatic genetic rescue in patient 1.** (A) White blood cells
 700 (WBC, triangles), hemoglobin (Hgb, circles) and platelets (diamonds) plotted over 23 years for patient 1
 701 (P1, pedigree 1). Red arrow indicates time of clinical presentation. (B) Illustration of germline RPA1
 702 variant in exon 9 and somatic mutation in exon 16 with respective DNA Sanger electropherograms from
 703 bone marrow. Bottom table depicts variant allelic frequencies from exome sequencing performed in
 704 bone marrow and skin fibroblast DNA and RNA sequencing from bone marrow at 20 years of age. (C)

705 Copy number neutral uniparental isodisomy (UPD) encompassing *RPA1* locus at 17p13.3 (red arrow)
706 identified using single nucleotide polymorphism (SNP) array. Serial SNP-array analysis in bone marrow
707 granulocytes demonstrates UPD expansion over time (denoted by purple brackets). (D) Schematic of
708 *RPA1* locus (grey bar) with germline (c.718) and somatic (c.1735) mutational spots 17kb apart. Three
709 haplotype orientations between c.718 and c.1735 identified in marrow DNA of P1 at age 19 years from 2
710 independent experiments using digital droplet PCR: left haplotype, wt/wt (c.718G wild type/c.1735G
711 wild type) denoted by black boxes; middle haplotype, mut/wt (c.718A mutant/c.1735G wild type)
712 denoted by green and black boxes; right haplotype, mut/mut (c.718A mutant/c.1735T mutant) denoted
713 by green and red boxes. (E) Ultradeep amplicon sequencing of bone marrow DNA and RNA targeting
714 position of *RPA1* somatic mutation (c.1735) confirms near total loss of mutant RNA. (F) Longitudinal
715 deep sequencing in bone marrow samples from diagnosis to age 25 years showing decrease in allele
716 frequency of the germline c.718G>A variant (red line) and increase of the somatic c.1735G>T mutation
717 (blue line). (G) Single cells from P1 bone marrow at ages 13 and 17 were sequenced for germline
718 (*RPA1*:chr17:1782314:G>A) and somatic (*RPA1*:chr17:1798378:G>T) mutational positions using single
719 cell (sc) DNA sequencing Tapestry platform. Violin plot shows 3 clonal populations including,
720 homozygous wild type (blue, $RPA1^{WT/WT}$, rescue clone 1 = UPD17p), heterozygous $RPA1^{E240K/WT}$ (gold,
721 native state hematopoiesis) and heterozygous c.718G>A with concurrent c.1735G>T stop-gain (red,
722 $RPA1^{E240K/WT + K579*}$ = rescue clone 2). (H) Tapestry single cell multi-omic analysis combining DNA mutation
723 data and surface protein expression performed in P1 bone marrow at age 17 years. Panels depict 3
724 clones (color coding identical to panel G) constructed from 2,110 high quality cells with normalized
725 protein expression of markers for hematopoietic stem and progenitor cells (CD34), stem cells (CD90),
726 progenitors (CD38), and terminally differentiated cells including, myeloid (CD11b), B-lymphoid (CD19)
727 and T-lymphoid (CD3) cells.

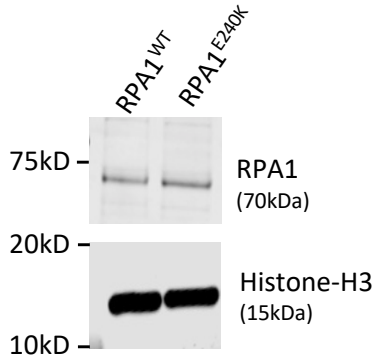




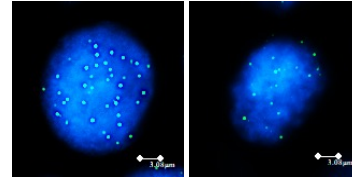
A



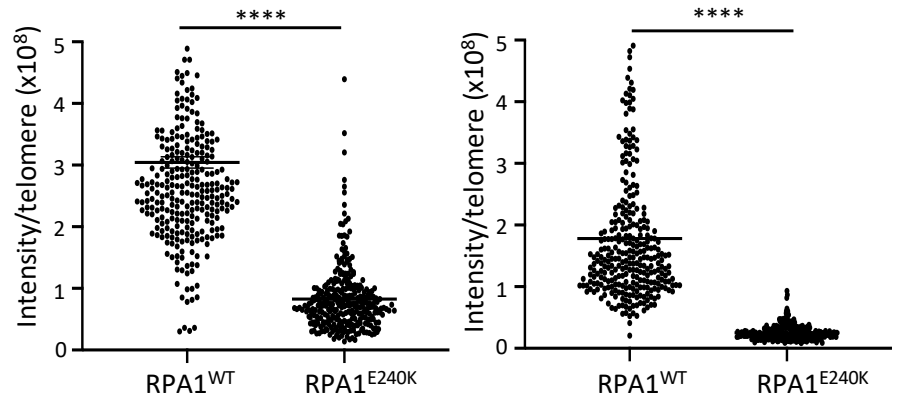
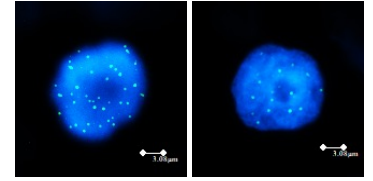
B



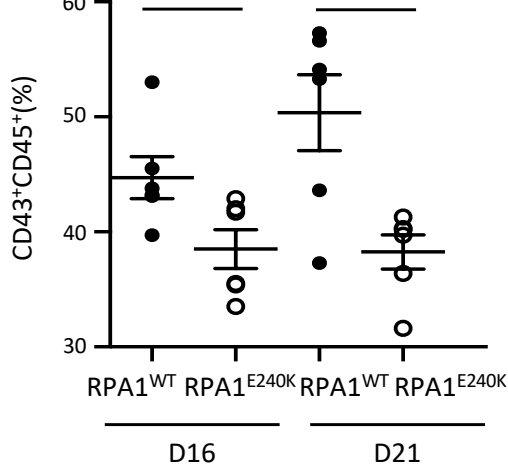
C



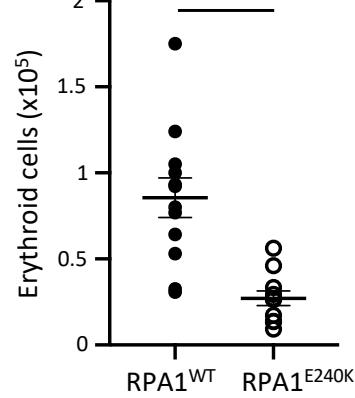
D



E



F



G

